



Article

# Electric Trolley Prototype for Goods and People Transport on Ziplines

Ettore Bianco <sup>1,\*</sup> , Claudio Giannuzzi <sup>2</sup>, Andrés Felipe Corredor Pablos <sup>2</sup>, Vicente Alfredo Peña Reyes <sup>2</sup> and Davide Berti Polato <sup>2</sup>

<sup>1</sup> Department of Mechanical and Aerospace Engineering, Politecnico di Torino, Corso Duca degli Abruzzi, 24, 10129 Turin, Italy

<sup>2</sup> Beond Srl, 10095 Grugliasco, Italy; claudio.giannuzzi@beond.net (C.G.); felipe.corredor@beond.net (A.F.C.P.); vicente.pena@beond.net (V.A.P.R.); davide.bertipolato@beond.net (D.B.P.)

\* Correspondence: etto.re.bianco@polito.it

**Abstract:** The increasing demand for efficient and cost-effective transportation solutions has led to the exploration of unconventional modes of transportation, such as ziplines. This paper presents the development of an electric prototype for a trolley that can be used for the simultaneous transport of goods and people on ziplines. The prototype is designed with a modular system that allows for easy customization based on the cargo's weight and size. Two lightweight Maxon motors have been integrated for traction purposes with two Maxon inverters and a low-voltage swappable battery pack. The trolley's chassis is made of lightweight materials, such as aluminum, making it highly maneuverable and capable of traveling at high speeds. The lightweight permits the operators to detach the trolley from the zipline when needed. The prototype's traction and braking systems are controlled through a user-friendly interface, making it easy to operate, and with the possibility of a robust and automatic routine for goods transport. In this article, we present the simulation for the design and testing of the prototype, as well as its potential applications in various industries, such as mining, agriculture, and emergency services. Our results show that the prototype is a viable solution for zipline-based transportation, with high efficiency and performance standards. Further research and development are being conducted to optimize the prototype's performance and expand its applications.



**Citation:** Bianco, E.; Giannuzzi, C.; Corredor Pablos, A.F.; Peña Reyes, V.A.; Berti Polato, D. Electric Trolley Prototype for Goods and People Transport on Ziplines. *World Electr. Veh. J.* **2024**, *15*, 100. <https://doi.org/10.3390/wevj15030100>

Academic Editor: Joeri Van Mierlo

Received: 30 January 2024

Revised: 26 February 2024

Accepted: 1 March 2024

Published: 6 March 2024



**Copyright:** © 2024 by the authors. Licensee MDPI, Basel, Switzerland. This article is an open access article distributed under the terms and conditions of the Creative Commons Attribution (CC BY) license (<https://creativecommons.org/licenses/by/4.0/>).

**Keywords:** prototype; electric trolley; zipline transport; motor control; brushless DC motor

## 1. Introduction

Zipline transportation systems are gaining significant attention in the transportation industry due to their potential to revolutionize goods and people transport, particularly in mountainous terrains and remote areas where traditional transportation methods are impractical or inefficient [1]. This paper presents a simulation, design, and production process for a prototype of a trolley for goods and people transport on ziplines. The paper provides an overview of the current state of zipline transportation systems, highlights the challenges and opportunities that exist, and presents the proposed solution. Traditional zipline transportation systems are based on the simple principle of using gravity to propel a trolley along a high-altitude cable [2–4]. The main issue with this system is the accumulation of trolleys at the end of the zipline and the need to bring them back to the top of the zipline. To do so, usually, traditional inefficient transportations are used, reducing the convenience of this kind of transport. The system has the potential to significantly reduce transport costs and time, particularly in areas that are difficult to access using traditional transportation methods. The system's reliability, efficiency, and sustainability make it an attractive alternative to traditional transportation methods. However, the technology is still in its early stages of development, and several challenges need to be addressed [5–7].

One of the main challenges in zipline transportation systems is the design of the trolley. The trolley needs to be lightweight, durable, and able to carry both goods and people. It also needs to have a high capacity for carrying payloads, be able to operate in different weather conditions, and be easily maintainable. The proposed solution presented in this paper addresses these challenges by developing a prototype trolley that meets the necessary requirements. The paper begins by highlighting the main challenges and opportunities that exist in zipline transportation systems. It then presents a detailed simulation process that was used to test the feasibility of the proposed trolley design. The simulation process involved the use of MATLAB/Simulink 2023b modeling software to test the trolley's performance under different conditions, including different weather conditions, cable angles, and payload weights. The simulation results provided valuable insights into the trolley's performance, which were used to refine the design and make necessary adjustments. Following the simulation process, the paper presents the design and production process for the prototype trolley. The design process involved the use of computer-aided design (CAD) software (Autodesk Inventor Professional 2024) to create a detailed 3D model of the trolley. The model was then used to create a physical prototype using a combination of traditional and modern manufacturing techniques. The production process involved the use of a 3D printer to create some of the trolley's components, such as the trolley plastic cover, while traditional manufacturing techniques were used to create other components, such as the trolley's frame. The paper concludes by presenting the results of the prototype's testing, which included range tests, torque tests, and speed tests. The tests provided positive results, demonstrating the prototype's feasibility and performance. In conclusion, this paper presents a simulation, design, and production process for a prototype of a trolley for goods and people transport on ziplines. The paper highlights the challenges and opportunities that exist in zipline transportation systems and presents a feasible solution for addressing these challenges. The simulation process, design process, and production process presented in this paper provide valuable insights into the development of zipline transportation systems and can serve as a guide for future research and development in this area.

The main article's contribution to the state of the art is the iterative design method of an electric trolley for zipline transport through a general vehicle model for fast prototyping purposes. The vehicle model has been validated and fitted to the experimental results to obtain a lightweight designed electric trolley.

## 2. Materials and Methods

Zipline transports have been used for many years for mountain transportation [8]. The principles behind this type of transport are related to the gravitational potential of the trolley at a higher altitude and its exploitation to produce kinetic energy. Most of the mountain environments are not compatible with a typical vehicle, so elevated metallic ropes are used to obtain a smooth path for a trolley, to reach the valleys. The typical rope transport is used only for the descent route, but the main issue with the only gravitational transport is the accumulation of the trolleys in the valleys and the consequent need for trolley transportation back to the top of the mountain with other ways of transport.

In this section, the design simulation is presented and explained. A MATLAB/Simulink simulation is used to design the trolley powertrain based on the mission constraints. The main output of the simulation is the powertrain sizing, including motors, inverters, and battery pack. The CAD simulation for the sizing evaluation is presented and analyzed.

### 2.1. Zipline Transports Current Solutions

Nowadays, the traditional zipline transports are the so-called gravity goods ropeway (GGR), for example, in mountainous territories such as Nepal or other mountainous territories [9–13]. Typically, GGR transport is a non-motorized way of transportation that moves goods from the top of the mountains to the valley by means of gravity. The Zipline GGR structure is made up of a metallic rope with two pulleys to sustain two trolleys during the whole route; two stations are needed uphill and downhill with the speed control pulley

and the brake system. The loaded trolley goes down, through gravity, moving uphill to an empty trolley that will be used for the next transportation after being loaded with new goods. The brake system is positioned to the downhill pulley to stop the trolley movement by means of an operator, when needed.

Recently, the use of ziplines has gained interest in the entertainment sector [14]. The ziplines are spreading to many tourist destinations all over the world. The trolley riders experience fast accelerations during the descent on the ziplines made up of a single rope without pulleys to support the trolley sliding down to the valley, typically at relatively high speed with the passenger tied to it. In this configuration, the brake has to be on the trolley, and it is common for the centrifugal brake to act when a certain speed is reached, so the final speed is fixed [15]. The choice of the trolley's maximum speed is fundamental for passenger safety, and it has to be calibrated with the spring at the end of the rope in order not to exceed the maximum acceleration, chosen not to be uncomfortable for riders, during the final deceleration. The main issue with having a single rope is present when the trolley has reached the valley at the end of the route; the system itself does not include the possibility of taking the trolley back to the start of the route without using other means of transport such as traditional vehicles taking back trolleys at the end of the day through mountain roads. This solution is quite inefficient, especially for mountain territories and ziplines longer than several hundreds of meters. The article proposes another possible solution by adding, to a typical passive trolley moved through gravity, an electric powertrain in order to have the possibility to go back uphill on the zipline. The electric-powered trolley can be used by people to rise back the zipline after the route or to take back the traditional trolleys accumulated at the end of the zipline during the day. In this work, the electric trolley design choices are explained, and the trolley model is validated through experimental tests.

The starting point for this collaboration is the gravity trolley with a self-integrated centrifugal magnetic brake manufactured by Adrenaline Constructions company. The challenge is to create an electric trolley capable of transferring power to the two wheels in Figure 1.



**Figure 1.** Gravity trolley from Adrenaline Constructions company.

## 2.2. Prototype Modeling for Optimal Design

In this subsection, a design model is set up for the trolley sizing. The project targets are the key factor for the trolley design, and they are shown in Table 1. This project's constraints are related to the longest ziplines installed by the company, and so the trolley must be

designed to travel it, in the worst case, with the maximum payload. The payload constraint is a desideratum of the company; it has been calculated by summing the gravitational trolleys' weight typically used in a working day on the zipline, and these trolleys need to be brought back to the top of the zipline by the electric trolley. The maximum trolley weight constraint has been considered taking into account the standard ISO 11228 [16] in which the maximum weight, liftable by an operator, is 25 kg.

**Table 1.** Project targets.

Target	Value	Unit of Measure
Slope profile	Catenary	-
Rated slope	23	[%]
Maximum slope	60	[%]
Maximum speed	7	[m/s]
Minimum average speed	3	[m/s]
Min distance	1500	[m]
Max distance	6000	[m]
Number of spans	6 (1500 m each)	-
Maximum trolley weight (without battery pack)	25	[kg]
Maximum battery pack Weight	10	[kg]
Payload	50	[kg]
Maximum mission time	10	[min]
Temperature working conditions	-20 ÷ 50	[°C]

The peculiarity of the project is the possibility of lifting the trolley by an operator and changing the span because the trolley has been designed to be integrated into the existing infrastructures, which have different lengths and numbers of spans. In Figure 2, an example of zipline configuration is shown, in which there is the starting point uphill and the finish point downhill; the path is divided into 3 segments made up of single-line ziplines connecting each station.

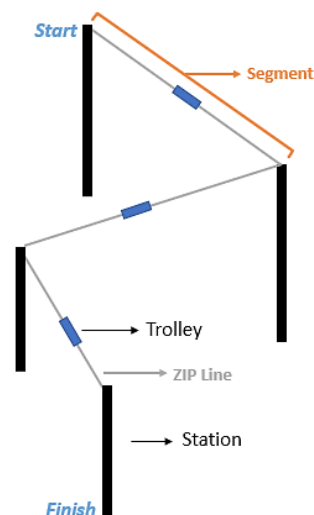


**Figure 2.** Zipline configuration example.

The project targets have been used to build up a comprehensive trolley model with the final goal of sizing its electromechanical characteristics. In Figure 3, the catenary shape [17] of the worst-case scenario of a 1500 m catenary is shown.

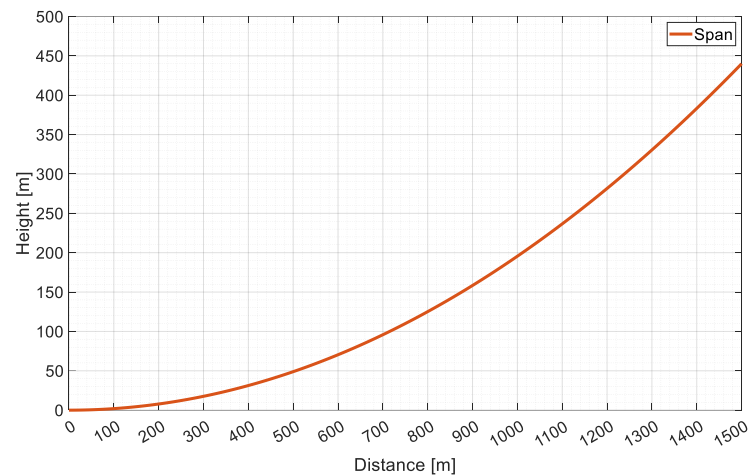


**Figure 3.** Zipline span height versus maximum target distance.

The speed reference has been generated considering time and weight constraints: the passenger must not wait on the trolley for more than 8 min, and the power has to be as low as possible in order to keep the lighter weight possible. Due to these two constraints, the model speed reference is set to an indicative value, through which the time constraint is not violated and the model generates the effective speed due to trolley characteristics. In Figure 4, a simulation example is reported with a reference speed set to 5 m/s and a ramp to reach 4 m/s in the final part of the zipline, due to power limitations on the maximum slope. In the example, the powertrain has been limited to 1 kW and the electric motor has been limited to 6000 rpm, reaching, with a gear ratio of 8, a trolley maximum speed of about 3.5 m/s before the flux weakening control begins to decrease the speed.

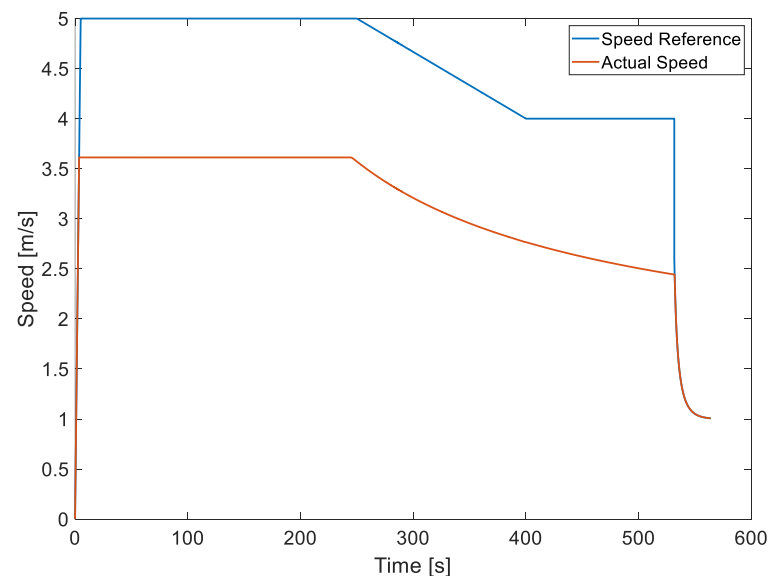


**Figure 4.** Speed reference compared with actual speed reached by the trolley limited to 1 kW.

A general vehicle energetic model [18] has been developed and implemented in the MATLAB/Simulink environment for the trolley design (Figure 5). In that model, some trolley parameters can be chosen, such as the wheel radius, vehicle mass, gear ratio, mechanical coefficients, powertrain efficiencies, electrical and mechanical limits, and so on. In Figure 6, a 4-motor trolley setup is shown with an electric motor speed limitation of 4500 rpm and a power limitation of 600 W, with a total mass of 105 kg.

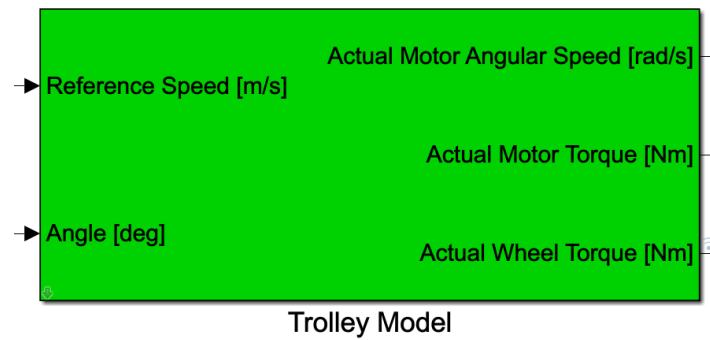


**Figure 5.** Customizable Simulink trolley model for design purposes.

TRACTION MODEL (mask)	
Parameters	
Wheel Radius [m]	0.046
Vehicle Mass [kg]	105
Hor distance of CG from front axle [m]	0.12
Hor distance of CG from rear axle [m]	0.12
CG height (wheel radius excluded) [m]	0
Friction coefficient [-]	0.3
Friction Safety Factor [-]	1.7
Number of traction wheels [-]	2
Rolling Resistance Coefficient $f_0$	0.01825
Threshold Speed [m/s]	0.01
Rolling Resistance Coefficient K	0
Vehicle Frontal Section [m <sup>2</sup> ]	2
Aerodynamic Drag Coefficient	1
Gravity Acceleration [m/s <sup>2</sup> ]	9.81
Speed Gear - Transmission Ratio	8
Climb Gear - Transmission Ratio	8
Gear change time [s]	240
Number of motors in the PWT [-]	4
Motor Maximum Power [W]	600
EM Maximum Speed [rpm]	4500
GearBox Efficiency	0.9
Electric Motor Efficiency	0.9
Inverter Efficiency	0.9

**Figure 6.** Customizable Simulink Mask for user parameters changes.

The energetic model is based on a speed controller, visible in Figure 7, for speed reference tracking. The block inputs are the speed error and the actual speed; the speed error is the input of the Proportional Integral (PI) regulator, and the actual speed is used for the torque saturation after the PI regulator, when the torque-speed motor map is available. The block outputs are the motor torque and the motor speed.

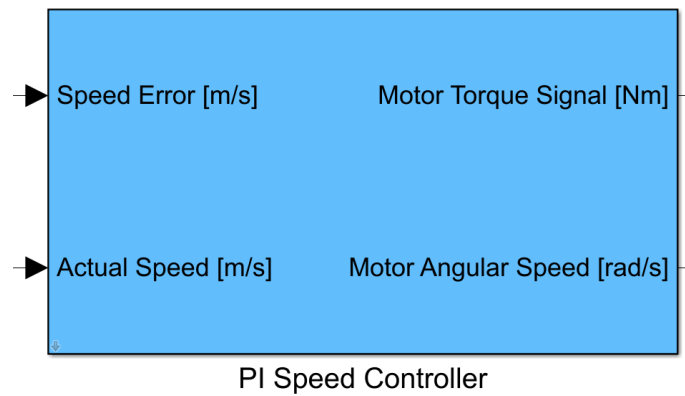


Figure 7. Speed controller based on PI regulator.

The speed controller is based on a PI regulator (Figure 8), combining a proportional gain and an integral gain for an optimal behavior on transients and to guarantee zero speed error at steady state.

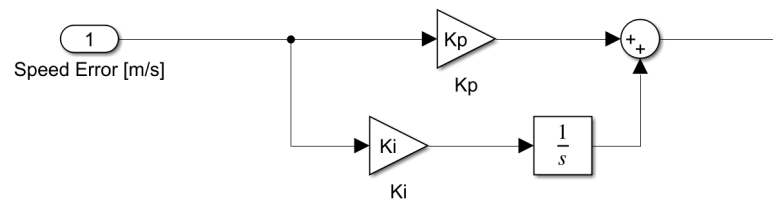


Figure 8. PI regulator blocks for speed control.

The choice of the PI regulator has been made in comparison with the model predictive control (MPC) [19]. The MPC, if properly tuned, can have a better step response, as evaluated in [20], concerning the PI controller. The main reason for the PI regulator choice is the tuning ease with respect to the MPC, especially in experimental applications.

The vehicle’s total resistive force has been taken into account to find out the power needed for the vehicle’s mission. Three force components have been considered: the aerodynamic force, the rolling resistance force, and the gravity force component due to the slope. Then, the total resistive force is converted into torque, and applied to the wheel, through the wheel radius. In Figure 9, the Simulink blocks are reported.

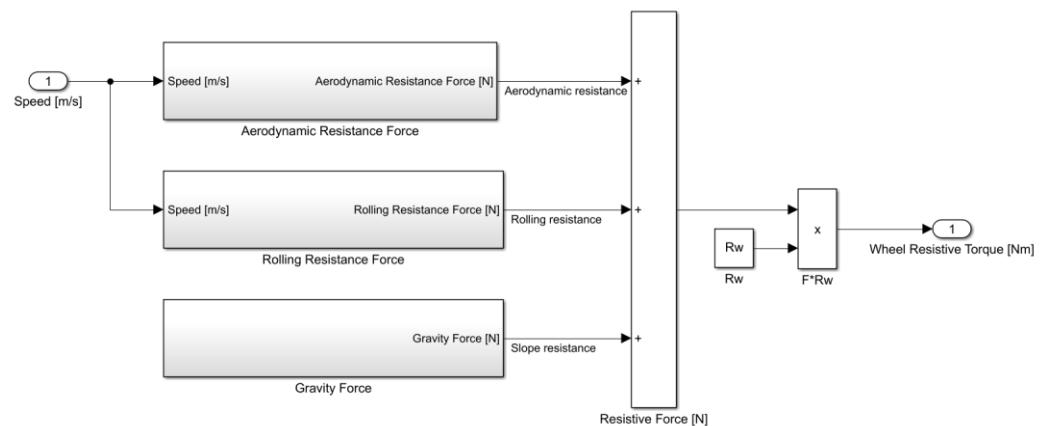


Figure 9. Resistive forces on the vehicle.

The three resistive force components ( $F_a$ ,  $F_r$  and  $F_g$ ) are computed through the following Equations (1)–(4), in which:

- $F_a$  is the aerodynamic force and it is dependent on the air density  $\rho$ , the vehicle frontal section  $S$ , the aerodynamic coefficient  $C_x$  and the speed squared  $v^2$  (1);

- $F_r$  is the rolling resistance force, proportional to the vehicle mass  $M$ , the gravitational acceleration  $g$ , the sum of  $f_{0,real}$  with the product between  $K$  and the speed squared  $v^2$ , and the cosine of the slope angle  $\alpha$ . The constants  $K$  and  $f_{0,real}$ , depending on  $f_0$  and  $v_{thresh}$ , are obtained from experimental tests, by fitting the experimental curves, performed by the company on the particular wheel geometry on the metallic rope.
- $F_g$  is the gravity force component acting on the trolley in the direction parallel to the ground, and it depends on  $M$ ,  $g$  and the sine of the slope angle  $\alpha$ .

$$F_a = \frac{1}{2} \cdot \rho \cdot S \cdot C_x \cdot v^2 \tag{1}$$

$$F_r = M \cdot g \cdot (f_{0,real} + K \cdot v^2) \cdot \cos(\alpha) \tag{2}$$

$$f_{0,real} = f_0 \cdot \tanh(v/v_{thresh}) \tag{3}$$

$$F_g = \frac{1}{2} \cdot M \cdot g \cdot \sin(\alpha) \tag{4}$$

Having obtained the resistive losses, the powertrain component losses have been calculated with preliminary reasonable fixed efficiencies to be substituted with the ones of the chosen components. In Figure 10, the vehicle energy from the energy stored in the battery pack to the vehicle kinetic energy is shown.

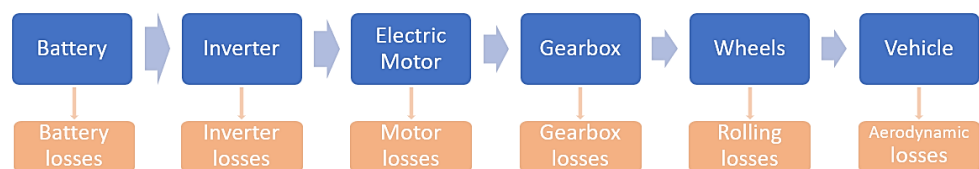


Figure 10. Electric powertrain energy flow.

For what concerns the battery pack, a complete model, based on the single-cell model, has been developed; the Simulink model is visible in Figure 11. The block input is the battery power output requested from the battery pack to complete the mission, and the block outputs are the battery voltage, the battery State Of Charge (SOC), and the battery current. It is mandatory to run the model, insert the cell capacity, the number of series and parallel in the mask. So, the block outputs are calculated by scaling the quantities of the single-cell model.

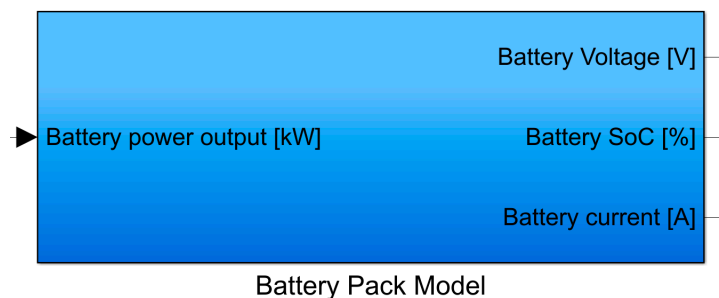
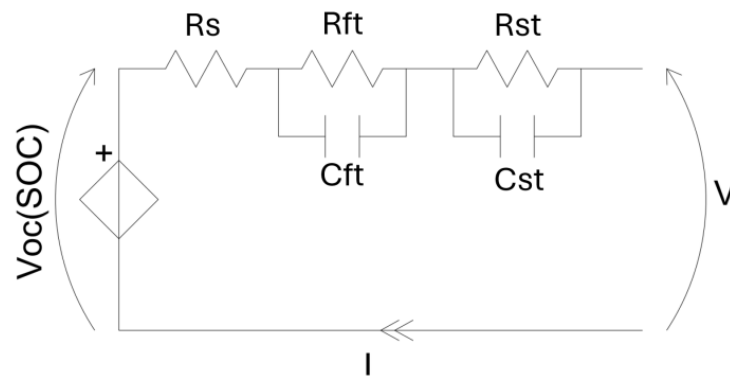


Figure 11. Resistive forces on the vehicle.

The single-cell model, on the base of the battery pack model, is a 2nd order Thevenin circuital model; the electric circuit is shown in Figure 12. The electric circuit is composed of the piloted voltage generator, which generates the open circuit voltage  $V_{oc}$  dependent on the SOC, the series resistance  $R_s$ , and two R-C circuits for the slow (fast transient resistance  $R_{st}$ , slow transient capacity  $C_{st}$ ) and fast transients (fast transient resistance  $R_{ft}$  and fast transient capacity  $C_{ft}$ ). From this model, it is possible to obtain the battery cell voltage  $V$  and current  $I$ . The circuit parameters have been obtained through experimental activities on the cylindrical cells used for the battery pack prototyping by Beond company.



**Figure 12.** Second-order Thevenin model [21].

### Powertrain Sizing

The model described in Section 2.2 has been used, first, without torque and power limitations, to define the powertrain components' sizing to reach the mission targets.

The model has been set with the project targets explained in Section 2.2. The model outputs have been evaluated to choose the components' characteristics; in Figure 13, the power, requested from the vehicle to carry out the mission profile, is shown. The maximum power of 2.23 kW is reached at the final part of the mission profile, when the slope is at its maximum value of about 30°. Without limitations on the powertrain's components, the time taken for the 1500 km path is less than 400 s, which means about 7 min, under the project time target.

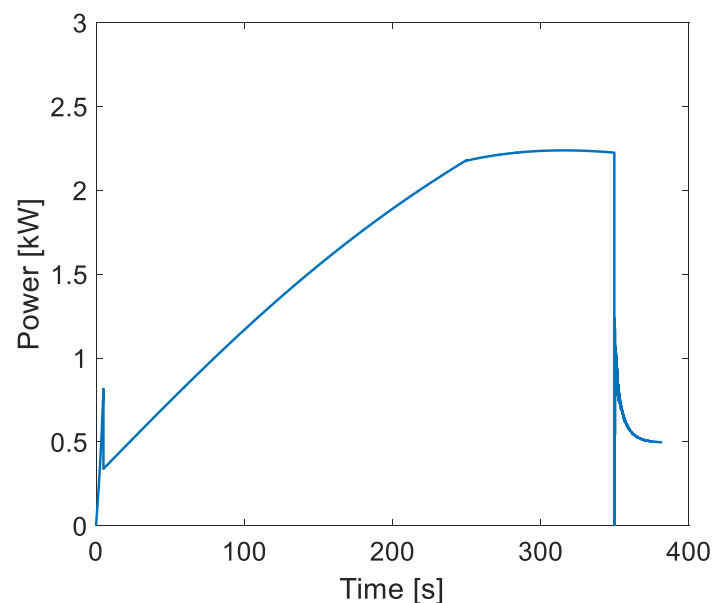


**Figure 13.** Power versus time during the trolley mission.

In Figure 14, the motor angular speed trend, during the mission, is visible, with a maximum value of about 8300 rpm.

The trolley gear ratio is fixed to 8 due to mechanical project choices, so the wheel torque is circa 8 times the motor torque. In Figure 15, the wheel torque (blue) and the motor torque (red) are shown: the maximum torque requested from the motor is about 3 Nm, and the wheel torque needed is about 23 Nm. Also, in this figure, the maximum value of the torque is requested at the final part of the mission when the slope is maximum.

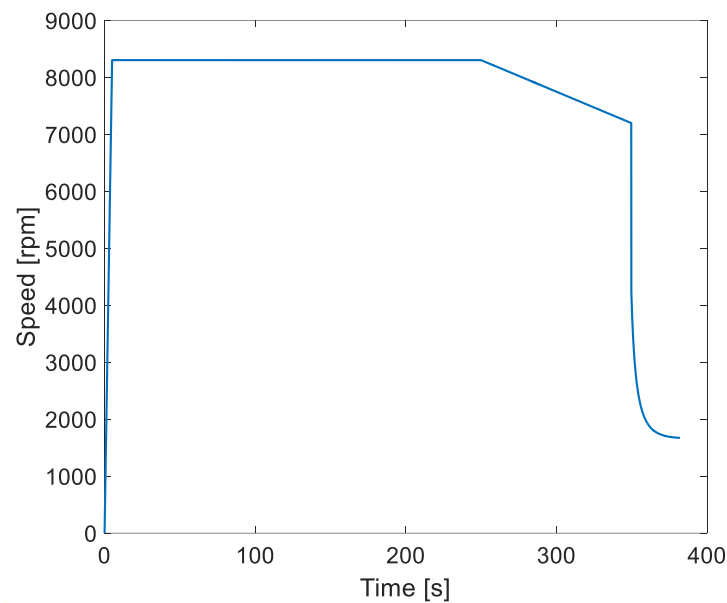


**Figure 14.** Motor angular speed versus time during the trolley mission.

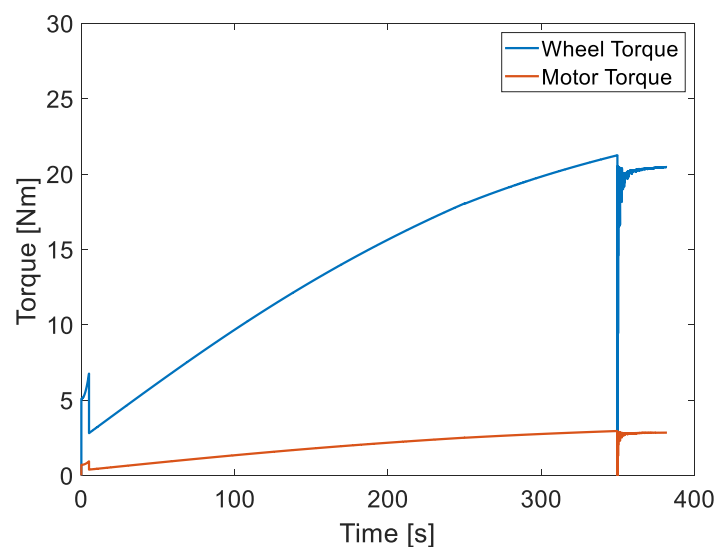


**Figure 15.** Motor torque versus time during the trolley mission.

With power, torque, and speed, it is possible to size the electric motor and the inverter to carry out the mission profile.

For the battery pack sizing, one of the key model outputs is the energy consumption for one span of 1500 m. In Figure 16, the wheel power is compared with the battery power that exceeds 3 kW because of the powertrain efficiencies; in the lower part of Figure 16, the cumulative energy consumption is shown, and it reaches 231 Wh for the 1500 m span.

The energetic model has been iteratively run with different battery pack configurations, in terms of cell series and parallels, in order to achieve the required autonomy. The final iteration has been simulated with a battery pack configuration of 12 series and 10 parallels of 2.5 Ah cylindrical cells. In Figure 17, the battery pack's main parameters can be seen: the battery voltage decreases from 50 V to about 45 V with a spike at the end of the span because the speed reference goes to zero, so the kinetic energy is regenerated to the battery pack, increasing the voltage; the battery SOC decreases from 100% to 80%, guaranteeing at least the autonomy of 5 spans 1500 m long; and the battery current reaches its maximum value of 70 A at the maximum span slope.

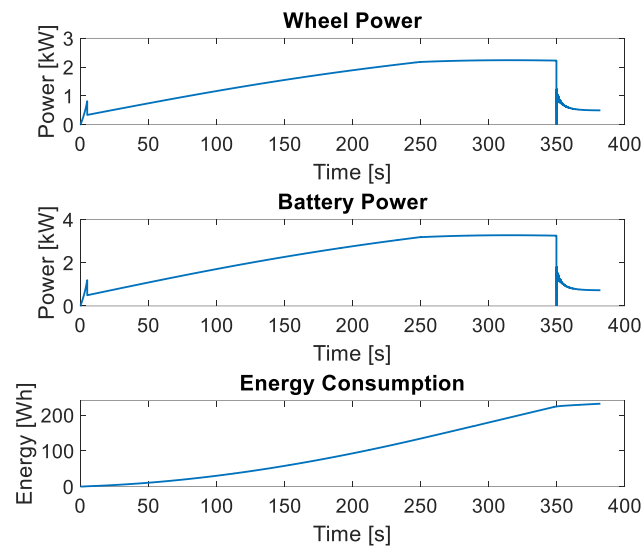


**Figure 16.** Wheel power (**up**), battery power (**center**), and energy consumption (**down**) for the 1500 m span.

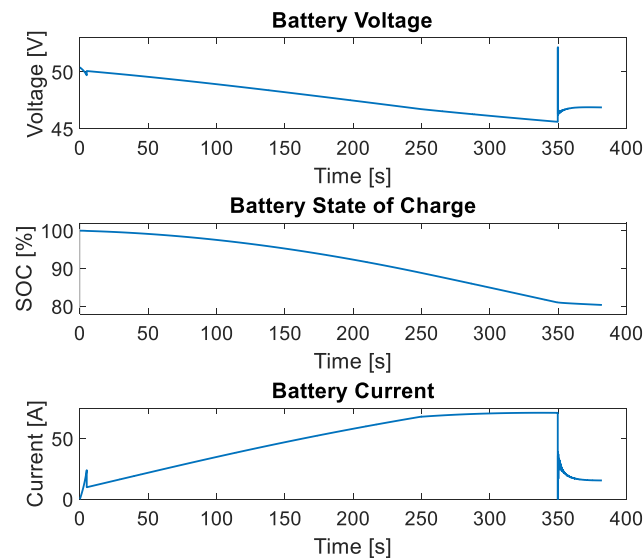


**Figure 17.** Battery voltage (**up**), battery state of charge (**center**), and battery current (**down**) for the 1500 m span.

Due to the challenging constraints, the sizing safety factor had to be as small as possible, avoiding the mass addition to the trolley.

### 2.3. Electric Trolley Fast Prototyping

After the powertrain sizing, the powertrain component choice has been carried out in order to meet all the project constraints. On the base of the components' choice, all the structural parts have been designed and manufactured, optimizing weights and volumes. The prototype described in this article is a first proof of concept, so all the choices made have been carried out also to minimize trolley production time.

#### 2.3.1. Battery Pack Prototyping

The battery pack is made up of single submodules from a commercial solution. The submodules have been connected in series to reach the voltage needed by the inverter and the electric motor. This architecture has been chosen because of the easy and fast connections among submodules conducted through busbars fixed by screws on the top of

the submodules. Moreover, this solution eases the battery design and its serviceability. The submodule, visible in Figure 18, is composed of 10 cylindrical 2.5 Ah cells connected in parallel, obtaining a total of 25 Ah of the submodule capacity.



**Figure 18.** 25 Ah battery pack module.

In Figure 19, the battery pack components are shown. A customized power board has been used to connect the submodules, integrating the busbars in the board, obtaining a single component, maintaining the submodules more fixed with respect to a single busbar for each connection. The other components needed are the contactor to guarantee the absence of voltage to the inverter DC-link when the battery pack is off, the shunt sensor, with the three voltage measurements on the two contactor poles and after the fuse, to know when a fuse trip happens and one current measurement, and the master-slave BMS boards for the battery pack management for safety and performance purposes.

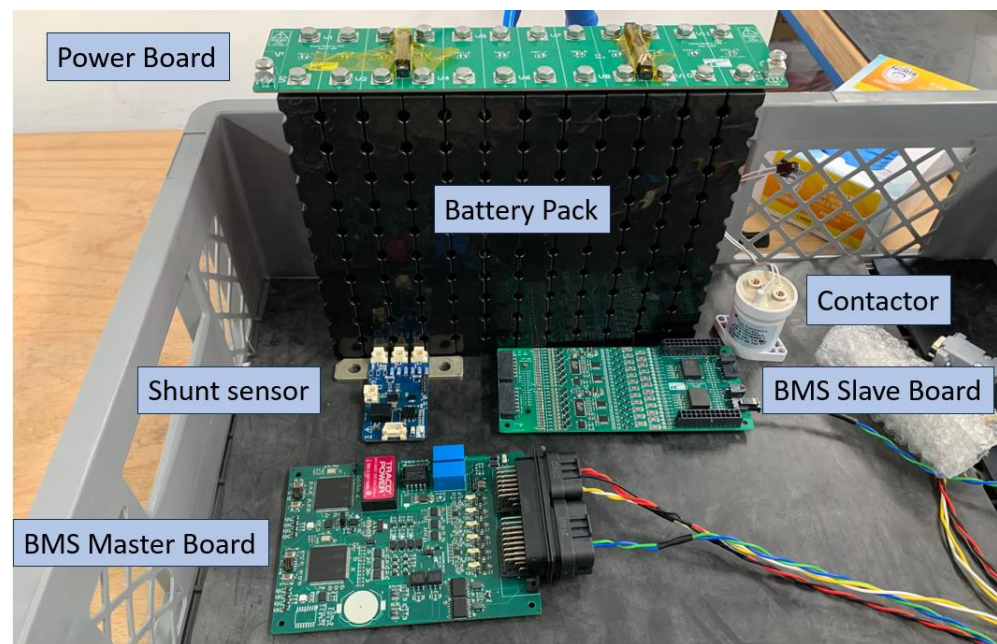


**Figure 19.** Battery Pack components: Modules, contactor, shunt sensor, BMS master board, BMS slave board, power board.

All the battery pack components have been integrated into the battery pack case. In Figure 20, some other battery pack components are shown: the DC/DC converter for the auxiliaries' supply, the fuse connected to the contactor battery pack, and the Electronic Control Unit (ECU) board responsible for the trolley control and logic.

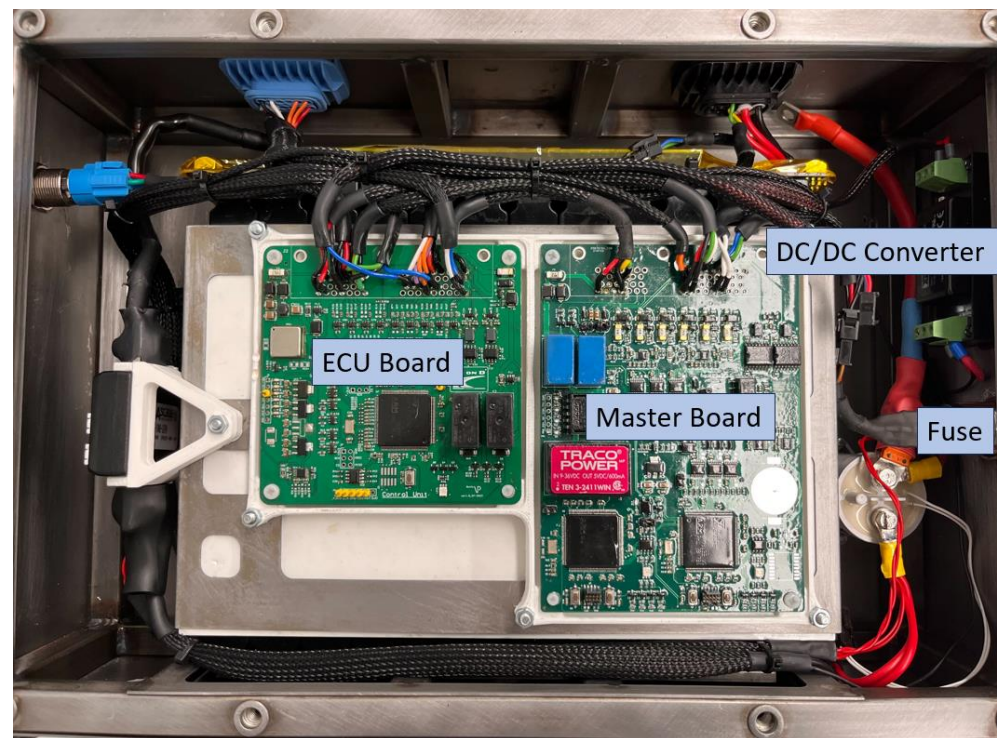


**Figure 20.** Battery pack assembly with the ECU board integration.

### 2.3.2. Drive Components Choice

The drive components have been chosen based on the power output of the energetic model. The best compromise between power and weight has been found in a flat Brushless DC outrunner motor [22], controlled by its designed inverter (Figure 21) [23].



**Figure 21.** Chosen motor (left) and the inverter (right).

To reach the requested maximum power of 2.23 kW, 4 flat motors are needed, because each motor can provide 600 W. For the first proof of concept, it has been decided to integrate 2 motors in the trolley to test the vehicle's capabilities, with a consequent halving of the maximum payload. It has been left to the possibility of integrating the other two motors into the structure to reach the target payload at a later time. In Figure 22, the torque-speed motor map, taken from the manufacturer datasheet, is shown. This map presents in red the motor's continuous operation, and it has been integrated into the motor torque saturator of the energetic model.

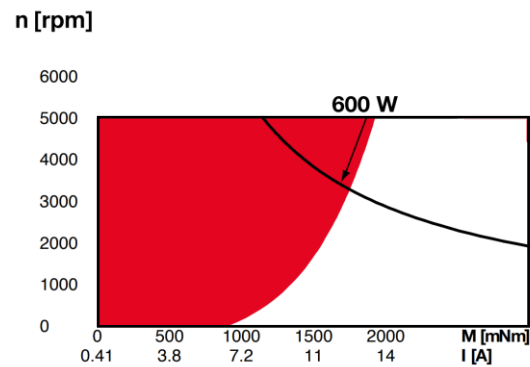


**Figure 22.** Torque/current-speed map from the electric motor datasheet with motor continuous operation region in red.

### 2.3.3. Mechanical Structure Production

All the trolley structural parts have been designed and produced to be as light as possible, but with enough strength to withstand the requested payload. The trolley structure is made up of two traction wheels directly connected to the toothed wheels of the gears. An additional freewheel has been inserted and connected to a lever to guarantee that the traction wheels have enough pressing force on the metallic rope, even on the maximum slope. The two motors have been connected to a central gear that transfers the torque from the two motors to the wheels with a gear ratio of 8. The wheels' material chosen is aluminum because of the mechanical strength sufficient for the application and the low weight. All the gears have been built in PEEK material to reduce the weight; the other structure parts have been built in steel because of the huge forces applied to the structures. The trolley geometry and materials have been chosen and verified with a first analytical evaluation in the worst-case load cases by solving the free body diagram and obtaining the lumped forces acting on key parts like the gears' teeth, bearings, and support flanges to which the load will be attached. Then a Fem evaluation has been carried out with Hypermesh 2023 in order to evaluate that the mechanical stresses were not greater than the materials' yield stress, as in [24]. The total CAD assembly is visible in Figure 23.

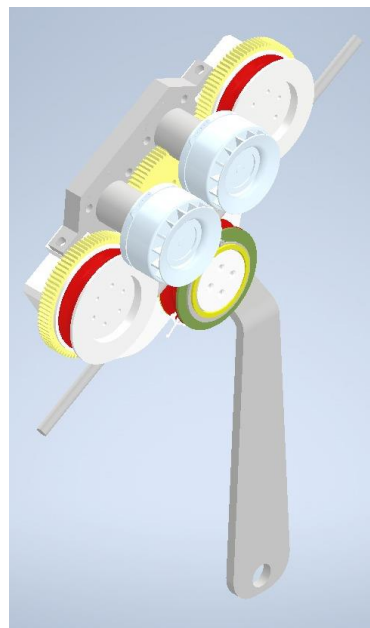


**Figure 23.** CAD assembly of the trolley traction structure.

A 3D-printed structure has been designed and produced to cover the rotating parts and the traction inverters. In Figure 24, the final traction structure is shown.



**Figure 24.** Trolley traction structure with 3D-printed cover.

The first trolley design was made with the battery pack attached to the flange under the rope to lower the structure's center of gravity. The battery pack has been integrated into a structural case capable of withstanding the payload; the material chosen was iron.

#### 2.3.4. Powertrain Control Integration

The powertrain control has been performed by the ECU board responsible for the reference generation [25] sent via Controller Area Network (CAN) to the inverters, and the block commutation motor control has been performed [23]. Being the motors in a mechanical parallel, it is not possible to perform a speed control for each motor because small differences can cause the instability of the control and could cause the motors to go one against the other. So, the inverters have been torque controlled, and a general speed control has been written in C language and performed by the ECU Board microcontroller, taking the feedback speed from one of the motors [26]. This approach is also valid when 4 motors are integrated.

The speed control used is a PI control with the proportional gain and the integral gain theoretically set through Equations (5)–(7), in which  $\omega_{speed}$  is the speed control bandwidth depending on the chosen frequency  $f_{sp}$  at least one decade less than the switching frequency to ensure control stability.  $k_{p,sp}$  is the proportional gain obtained with  $\omega_{speed}$  and the equivalent vehicle inertia  $J_{eq}$  seen by the motor, and the integral gain  $k_{i,sp}$  depending on  $\omega_{speed}$  and  $k_{p,sp}$ .

$$\omega_{speed} = 2 \cdot \pi \cdot f_{sp} \quad (5)$$

$$k_{p,sp} = \omega_{speed} \cdot J_{eq} \quad (6)$$

$$k_{i,sp} = \omega_{speed} \cdot k_{p,sp} \quad (7)$$

Then, the PI gains were experimentally tuned to obtain the optimal trade-off between control performance and stability. The final gains obtained are visible in Table 2.

**Table 2.** PI gains obtained.

Parameter	Value	Unit of Measure
Proportional gain	0.0747	[Nm/(rad/s)]
Integral gain	0.0023	[Nm]

The trolley control logic has the purpose of obtaining an automatic object, but with the possibility, for an operator, of interacting with the trolley. The trolley logic is explained in the flowchart of Figure 25: If the start button is pressed, the motor starts at slow speed, reading the colored bands on the rope that indicate the total rope length, and then the acceleration starts reaching the maximum target speed and then the maximum power available. When the final colored band is detected or the internal distance counter reaches

the total length of the rope, the trolley slows down at 1 m/s until the end-of-line sensor detects the stop station and stops the trolley.

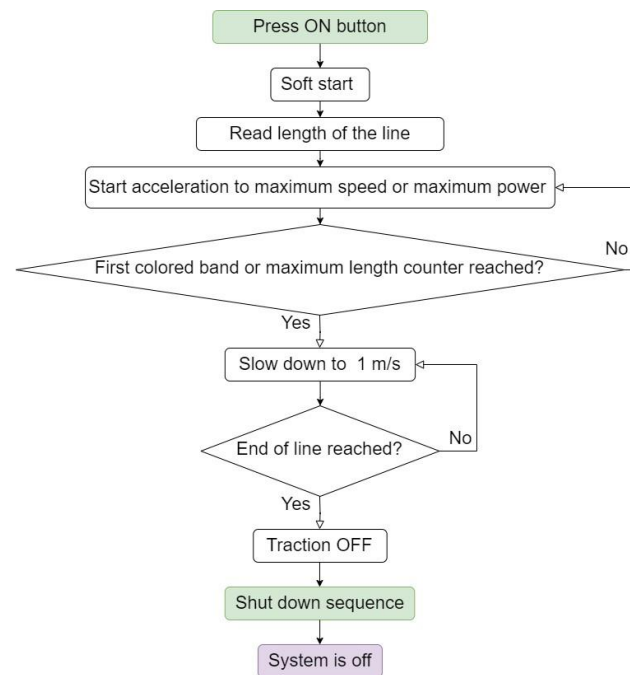


**Figure 25.** Trolley control logic.

For this prototype, the start, stop, and emergency buttons are fixed to a wired remote control usable by the operators. The green start button on the control side, the red stop button, and the emergency fungus, on the front of the controller are shown in Figure 26.



**Figure 26.** Wired remote control.

In Figure 27, the colored bars are shown, indicating the total rope length, detected by the SICK optic sensor [27].

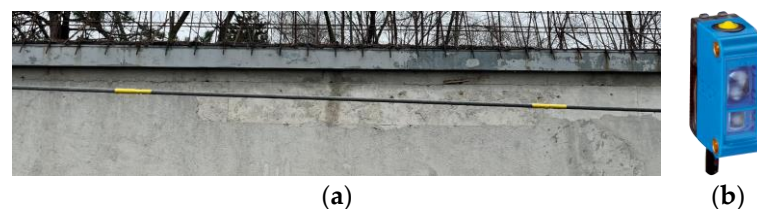


**Figure 27.** Colored band indicating the total length of the rope (a); optic sensor for colored bar detection (b).

The stop station is detected by the end-of-line sensors visible in Figure 28. When the station is reached, a mechanical block is needed to fix the trolley mechanically even if the emergency button is pressed.



**Figure 28.** Trolley traction structure with the end-of-line sensors mounted.

Since no mechanical brakes are present, when the trolley needs to stop, the motor control switches from speed control to position control, imposing a fixed motor angular position. Position control is very important at the end of the span when the slope is at its maximum and the trolley returns to the valley because of the weight force component parallel to the rope.

### 3. Results

In this section, the main experimental results are presented. The trolley was tested first with a bench test to verify the component integration and motor control, then the trolley was tested on a horizontal metallic rope to emulate the real environment and validate the control logic of the trolley automation. The final test was carried out in the final environment to evaluate the trolley's performance compared with the mission targets.

#### 3.1. Bench Tests

The bench test has been performed in the laboratory (Figure 29) without resistive torques on the motors. The main goal of the test is to validate the powertrain integration and the components' communication.



**Figure 29.** Bench test setup.

The main outputs of the test are reported in Table 3.

**Table 3.** Bench Test main results.

Tested Parameters	Value	Unit of Measure
Motor max torque	1 (software limit)	[Nm]
Motor max speed	4500 (voltage limit)	[rpm]
Communication delay	10	[ms]
BMS limits	OK	-
Inverter limits	OK	-
Control logic	OK	-
Measurements	OK	-

During the bench test, two strong limitations were discovered: the first is the motor torque limitation to 1 Nm compared to the datasheet motor maximum torque of 1.7 Nm; the second is the motor maximum speed of 4500 rpm instead of 5000 rpm in the datasheet. The first limitation is the most important because it can lead to the impossibility of reaching the top of the span. The second limitation can lead to a mission time duration higher than the target one. The communication between the ECU board and the inverters is via can, and in the bench test, the time delay between the command and the reference change has been measured, and it is 10 ms. The communication delay affects the control stability and dynamics, but the mission speed profile has been limited with speed ramps to ensure trolley control stability.

### 3.2. Horizontal Metallic Rope Tests for Control Logic Validation

A 100 m metallic rope has been fixed outside the laboratory to validate the trolley control logic in a realistic environment. The trolley has been tested in the final configuration (Figure 30) on a horizontal rope with different payloads.

**Figure 30.** Trolley in the final configuration.

The tests performed are the following:

- Maximum speed test
- Maximum torque test
- Payload test
- Range test

### 3.2.1. Maximum Speed Test

The test consists of an initial motor soft start at 500 rpm and then a speed ramp of 500 rpm/s until the motor reaches the maximum value possible. In Figure 31, the motor speed during the test is measured in rpm. The maximum speed reached is about 4500 rpm, limited by the inverter software Epos Studio 3.7 because of the motor's mechanical maximum speed of 5000 rpm. Because of the speed limitation, the maximum longitudinal speed reached by the trolley is 13.5 km/h.

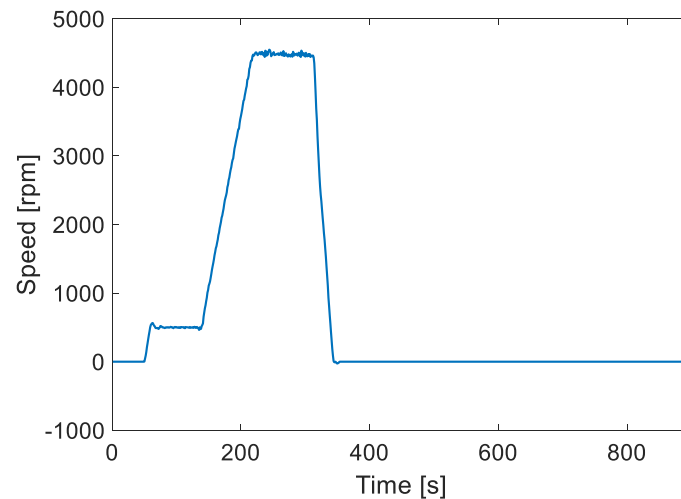


Figure 31. Speed profile during the maximum speed test.

### 3.2.2. Maximum Torque Test

The maximum speed test has been performed without a payload but by manually blocking the trolley during the accelerations. The test has been repeated in one direction and the other, so the first part of the test has positive speed and the second part is negative; the same is true for the torque. In Figure 32, the speed profile is visible, and, during the accelerations, irregular ramps can be noticed due to the manual interference adding resistive torque to the motors and evaluating the torque response. In Figure 32, it is visible that the torque has reached a maximum saturated value at 1 Nm, during the accelerations, due to a software Epos Studio 3.7 limitation because of the inverter board current limit.

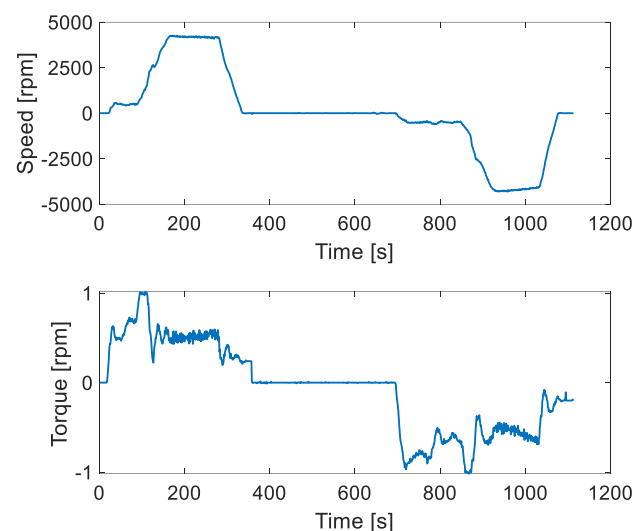


Figure 32. Speed profile during the maximum torque test (**up**) and torque profile during the maximum torque test (**down**).

### 3.2.3. Payload Test

The payload test has been performed with the addition of weights hanging from the battery pack case. The maximum weight added to the trolley is 55 kg due to the structural limits of the metallic rope supports. The trolley setup, with the weights attached to the battery pack with straps, is shown in Figure 33.



**Figure 33.** Electric trolley with 55 kg payload.

The payload test speed reference logic has been maintained the same as the maximum torque test, so the trolley starts the mission at 500 rpm and then accelerates to the maximum value of 4500 rpm. In Figure 34, the speed and torque, during the payload test, are presented: The test is performed in two directions, so positive and negative values of speed and torque are compared. The torque reached during the test is 0.6 Nm due to the payload, compared to 0.4 Nm without the payload.

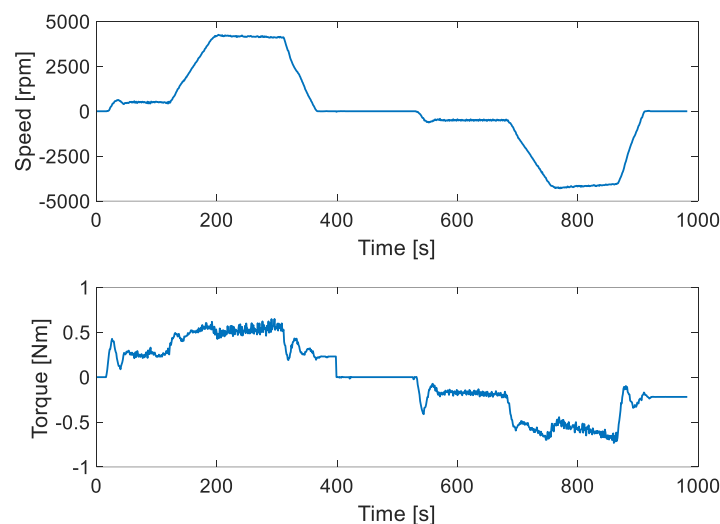


**Figure 34.** Electric trolley with 55 kg payload.

### 3.2.4. Range Test

A range test is needed to evaluate the trolley's autonomy. The test has been performed on the 100 m rope, repeating the mission until 2 km have been traveled. In Figure 35, the range test speed profile can be seen, with the metallic rope traveling 22 times in one

direction and 22 times in the opposite direction to reach 2 km. After the range test, the battery SOC was 3% less than at the beginning of the test, so the total autonomy reached on a horizontal rope without a payload is 66 km.

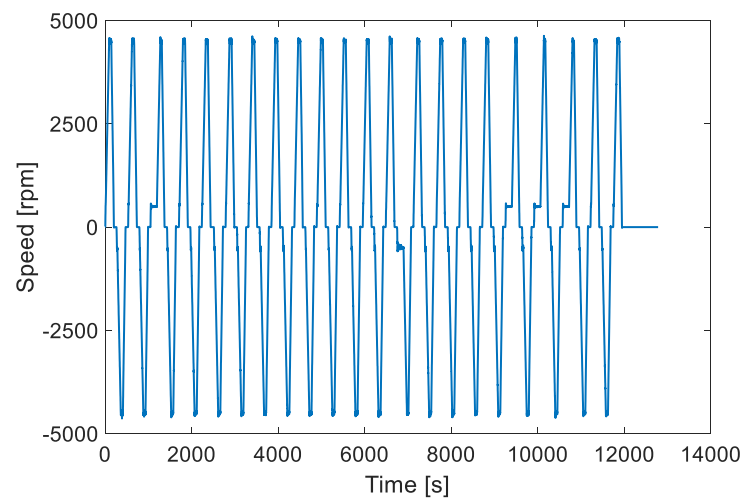


**Figure 35.** Range test speed profile to reach 2 km of path.

### 3.3. Experimental Tests on Final Application for Model Validation

Finally, the electric trolley has been tested in the final application environment. The experimental tests have taken place in Marebbe (BZ) on a real zipline with a maximum slope of 45%. The test has been performed with a reference speed of 1000 rpm, as shown in Figure 36, after the soft start at 500 rpm. The total distance covered on the zipline during the test is 80 m with an increasing slope until the maximum slope; the test has been repeated for three different payloads: 5 kg, 25 kg, and 45 kg. The torque requested from the motors has increased from 5 kg to 45 kg; the maximum torque requested from one motor in the 5 kg test is 0.8 Nm; for the 25 kg and 45 kg tests, the torque is saturated to 1 Nm. During the 25 kg tests, the trolley followed the speed reference until the end of the zipline; in the 45 kg test, the trolley could not follow the speed reference, visible in Figure 36 (yellow line of the central graph). The trolley reached the top of the zipline because of the operator, connected by a rope to the trolley, who pulled the trolley until the end of the zipline.

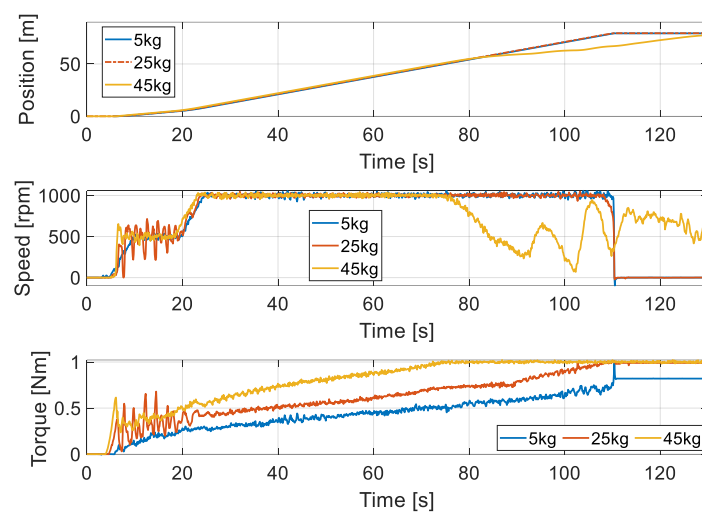


**Figure 36.** Trolley position (up), speed (center), and torque (down) during the experimental tests with different payloads: 5 kg, 25 kg, 45 kg.

Having obtained the experimental measurements, the model outputs can be compared to the experimental curves. The comparison is more meaningful for the 5 kg acquisition

because the torque is not saturated to 1 Nm. So, the experimental actual speed has been used as the model input speed reference, and the motor torque output has been compared to the experimental measured torque. The control dynamic has been regulated for a very high dynamic in order to guarantee that the actual speed will strictly follow the reference speed. All the other model parameters have been kept the same as the final trolley configuration. In Figure 37, the actual motor speed (up) and the torque comparison between the model and the experimental test (down) are shown.

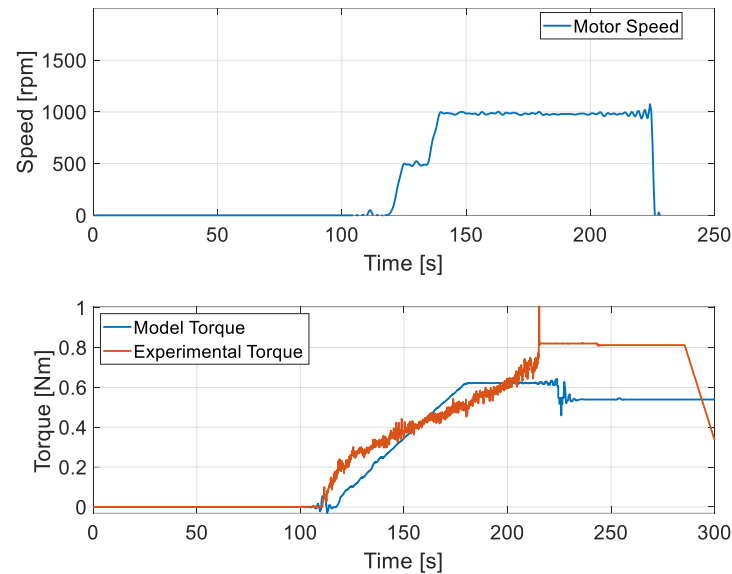


**Figure 37.** Trolley motor actual speed (**up**), torque comparison (**down**) between the model and the 5 kg experimental test.

It is important to notice that the experimental maximum motor torque is about 0.8 Nm, when the model has a motor torque output of 0.5 Nm in the test conditions. The model torque curve has been fitted iteratively, acting on the rolling resistance coefficient and on the gearbox efficiency, obtaining the values in Table 4. The rolling resistance coefficient obtained is 3 times higher than the original one considered originally in the model, and the gearbox is 0.8 instead of 0.9. This means that the sizing power has to be greater than the one previously calculated, due to the greater resistive forces seen by the powertrain.

**Table 4.** Parameters correction by experimental fitting.

Parameter	Original Value	Fitted Value	Unit of Measure
Rolling resistance	0.018	0.054	[Adim]
Gearbox efficiency	0.9	0.8	[Adim]

#### 4. Conclusions

In conclusion, an electric trolley prototype has been modeled, designed, and assembled. The sizing model has been implemented in MATLAB/Simulink to choose the powertrain components, simulating the zipline environment, to reach the project targets. The battery pack has been assembled, and two Maxon drives have been used for the trolley traction. The trolley prototype has been tested to validate the model. The control logic has been automated with three levels of redundancy: The internal distance counter, colored bands on the rope read by the optic sensors, and the end-of-line sensor to detect the final station. The experimental application has denoted a higher resistance force on the trolley, so, the model outputs have been fitted with the experimental measures. The fitted model can be used for the design of other prototypes with different targets.

This project underlines the feasibility of zipline transports of goods and people with electric trolleys, avoiding the need for high-cost powered stations, and with the possibility to ascend the zipline independently even on high slopes.

The model implemented has been experimentally validated after a fitting procedure, and it can be used for trolley design with different performance targets.

**Author Contributions:** Conceptualization, E.B. and D.B.P.; methodology, E.B., C.G. and V.A.P.R.; software, E.B., A.F.C.P. and V.A.P.R.; validation, E.B., A.F.C.P. and V.A.P.R.; formal analysis, E.B. and D.B.P.; investigation, E.B. and C.G.; data curation, E.B. and A.F.C.P.; writing—original draft preparation, E.B.; writing—review and editing, E.B.; supervision, C.G. All authors have read and agreed to the published version of the manuscript.

**Funding:** This research received no external funding.

**Data Availability Statement:** Data is contained within the article.

**Acknowledgments:** We would like to express our deepest gratitude to all those who have contributed to the completion of this article on zipline transports. First, we would like to acknowledge Adrenaline Constructions company for having commissioned the project and for having shared the technical experience on gravity trolleys and zipline structures. We would also like to extend our appreciation to Beond Srl for being the key partner of the project, for having led the project and for sharing the experience on the electrification field.

**Conflicts of Interest:** Claudio Giannuzzi, Felipe Andrés Corredor Pablos, Vicente Alfredo Pena Reyes, Davide Berti Polato are employees of Beond Srl. The other authors declare no conflicts of interest. The paper reflects the views of the scientists, not the company.

## References

1. Jojić, T.; Vladić, J.; Đokić, R. Specific machines and devices with horizontal rope as carrying element-zipline. *Proc. Fac. Tech. Sci.* **2018**, *33*, 13–16.
2. Jojić, T.; Vladić, J.; Đokić, R. Anchorage type and tension rope force impact on zipline's kinematic characteristics. *Mach. Des.* **2019**, *11*, 149–154. [\[CrossRef\]](#)
3. Steele, C.Z.; Udow, D.E.; Steele, R.L. Continuous Assist Zipline Braking and Control System. US Patent Application No. 2011/0162917 A1, 22 December 2011.
4. Đokić, R.; Vladić, J.; Jojić, T. Zipline computational model forming and impact of influential sizes. In Proceedings of the 7th International Conference “Transport and Logistics-TIL 2019”, Niš, Serbia, 6 December 2019; pp. 71–74.
5. Vladić, J.; Živanić, D.; Džinčić, I.; Đokić, R.; Gajić, A. Application of the numerical methods for dynamic analysis of transport systems with rope. In Proceedings of the VIII Triennial International Conference HEAVY MACHINERY-HM 2014, Zlatibor, Serbia, 25–28 June 2014; pp. 37–42, ISBN 978-86-82631-74-3.
6. Vladić, J. The Parametric of Equation of a Catenary Line and Theoretical Foundations for Static Analysis a Ropeway. In Proceedings of the XV European Conference of Material Handling Teaching Professors, Novi Sad, Serbia, 22–26 September 2004; pp. 170–178.
7. Jojić, T.; Vladić, J.; Đokić, R. Zipline Design Issues and Analysis of the Influencing Parameters on Passenger's Velocity. In Proceedings of the 5th International Conference “Mechanical Engineering in XXI Century-MASING 2020”, Niš, Serbia, 9–10 December 2020; pp. 129–132.
8. Vladić, J.; Jojić, T.; Đokić, R.; Gajić, A. Theoretical backgrounds for zipline analysis. In Proceedings of the XXIII International Conference on “Material Handling, Construction and Logistics-MHCL, Vienna, Austria, 18–20 September 2019. [\[CrossRef\]](#)
9. Kc, D.; Maraseni, T.; Jamir, C.; Magar, R.T.; Tuladhar, F. Effectiveness of Gravity Goods Ropeways in market. *Transportation* **2020**, *47*, 1393–1414. [\[CrossRef\]](#)
10. Magar, T.R. Gravity Goods Ropeways: A Sustainable Solution for Rural Transportation in Hilly and Mountainous Regions of Nepal. 27 October 2016. Available online: [https://scholarsbank.uoregon.edu/xmlui/bitstream/handle/1794/20424/ThapaMagar\\_oregon\\_0171N\\_11478.pdf?sequence=1](https://scholarsbank.uoregon.edu/xmlui/bitstream/handle/1794/20424/ThapaMagar_oregon_0171N_11478.pdf?sequence=1) (accessed on 30 January 2024).
11. Laxman, K.C. Gravity goods ropeway an alternative sustainable solution for rural transportation without hampering to the natural environment and climate: A case study from Janagaun village. *IOP Conf. Ser. Earth Environ. Sci.* **2009**, *6*, 202019. [\[CrossRef\]](#)
12. Adhikari, D. *Potential Development of Gravity Goods Ropeway Andits Impact on Rural Livelihood (A Case Study of Gholechappra Settlement at Bukhel VDC in Lalitpur District)*; Department of Rural Development: New Delhi, India, 2011.
13. Baral, L.B.; Nakarmi, J.J.; Poudyal, K.N.; Karki, N.R.; Nalmpantis, D. Gravity and muscle force operated surface ropeway: An efficient, cheap, and eco-friendly transport mode for mountainous countries. *Eur. Phys. J. Plus* **2019**, *134*, 55. [\[CrossRef\]](#)
14. Quizona, K.D.; Shelly, S.; Holman, N.; Glozer, M.; Black, A. Physical and digital architecture for collection and analysis of imparted accelerations on Zip Line attractions. *JTEAS J. Themed Exp. Attract. Stud.* **2018**, *1*, 61–65.

15. Jovan, V.; Tanasije, J.; Radomir, Đ. Condition analysis and basis for selection of zipline arresting devices. *IMK-14-Istraz. Razvoj* **2020**, *26*, 89–94. [[CrossRef](#)]
16. *ISO 11228-1:2021; Ergonomics—Manual Handling—Part 1: Lifting, Lowering and Carrying*. ISO: Geneva, Switzerland, 2021.
17. Such, M.; Jimenez-Octavio, J.R.; Carnicero, A.; Lopez-Garcia, O. An approach based on the catenary equation to deal with static analysis of three dimensional cable structures. *Eng. Struct.* **2009**, *31*, 2162–2170. [[CrossRef](#)]
18. de Carvalho Pinheiro, H. PERFECT Design Tool: Electric Vehicle Modelling and Experimental Validation. *World Electr. Veh. J.* **2023**, *14*, 337. [[CrossRef](#)]
19. Hu, Z.J.; Su, R.; Zhang, K.; Xu, Z.Y.; Ma, R.J. Resilient event-triggered model predictive control for adaptive cruise control under sensor attacks. *IEEE/CAA J. Autom. Sin.* **2023**, *10*, 807–809. [[CrossRef](#)]
20. Salem, F.M.; Mossad, M.I.; Awadallah, M.A. A comparative study of MPC and optimised PID control. *Int. J. Ind. Electron. Drives* **2015**, *2*, 242. [[CrossRef](#)]
21. Rizzello, A.; Scavuzzo, S.; Ferraris, A.; Airale, A.G.; Bianco, E.; Carello, M. Non-linear Kalman Filters for Battery State of Charge Estimation and Control. In Proceedings of the 2021 International Conference on Electrical, Computer, Communications and Mechatronics Engineering (ICECCME), Mauritius, Mauritius, 7–8 October 2021; pp. 1–7. [[CrossRef](#)]
22. Sensinger, J.W.; Clark, S.D.; Schorsch, J.F. Exterior vs. interior rotors in robotic brushless motors. In Proceedings of the 2011 IEEE International Conference on Robotics and Automation, Shanghai, China, 9–13 May 2011; pp. 2764–2770. [[CrossRef](#)]
23. Bianco, E.; Carello, M. A first e-scooter powertrain analysis for Fuel Cell integration. In Proceedings of the 2022 International Conference on Electrical, Computer, Communications and Mechatronics Engineering (ICECCME), Male, Maldives, 16–18 November 2022; pp. 1–6. [[CrossRef](#)]
24. Daoudi, K.; Boudi, E.M. Structural Investigation of the Gearbox with Epicyclical Gear System by FEM. In Proceedings of the 2018 International Conference on Electronics, Control, Optimization and Computer Science (ICECOCS), Kenitra, Morocco, 5–6 December 2018; pp. 1–5. [[CrossRef](#)]
25. Grano, E.; Lazek, T.; Carello, M. A numerical methodology for induction motor control: Lookup tables generation and steady-state performance analysis. In Proceedings of the WCX SAE World Congress Experience (WCX24) 2024, Detroit, MI, USA, 16–18 April 2024.
26. Liu, Y.; Zhao, J.; Xia, M.; Luo, H. Model Reference Adaptive Control-Based Speed Control of Brushless DC Motors with Low-Resolution Hall-Effect Sensors. *IEEE Trans. Power Electron.* **2014**, *29*, 1514–1522. [[CrossRef](#)]
27. Lataire, L. Optical Sensors for Factory Automation. In Proceedings of the Proceedings SPIE 0672, In Situ Industrial Applications of Optics, Brussels, Belgium, 22 July 1986. [[CrossRef](#)]

**Disclaimer/Publisher’s Note:** The statements, opinions and data contained in all publications are solely those of the individual author(s) and contributor(s) and not of MDPI and/or the editor(s). MDPI and/or the editor(s) disclaim responsibility for any injury to people or property resulting from any ideas, methods, instructions or products referred to in the content.